Research Article

Sonu Lamba and Prashant K. Srivastava*

Cost-effective optimal control analysis of a COVID-19 transmission model incorporating community awareness and waning immunity

https://doi.org/10.1515/cmb-2023-0154
received March 31, 2023; accepted June 26, 2023

Abstract: This article presents a cost-effective optimal control analysis of interventions applied to a S2EI2RS type deterministic compartmental model of COVID-19, considering community awareness and immunity loss. We introduce two time-dependent controls, namely, home quarantine and treatment, to the model for defining an optimal control problem (OCP). In addition to some basic qualitative properties, we obtain the reproductive threshold R_0 by using the next-generation method and see the impact of controls on it. We also investigate the effect of community awareness and waning immunity, when no controls are applied. The existence and characterization of optimal controls is proved to establish the optimality system, and the OCP is solved using the forward–backward sweep method. The results are simulated using MATLAB. Our comparative cost-effective analysis indicates that implementing both control strategies simultaneously, along with community awareness, is the most optimal and sustainable way to flatten COVID-19 curves in a short period of time than that of implementing single controls. This article offers valuable insights that can assist policymakers and public health experts in designing targeted and effective control measures for COVID-19 and future epidemics in the post-COVID era. Therefore, this piece of work could be a valuable contribution to the existing literature.

Keywords: optimal control, Pontryagin's maximum principle, forward–backward sweep method, cost-efficacy analysis

MSC 2020: 34H05, 49K15, 92B05, 92D30

1 Introduction and motivation to the research context

The COVID-19 pandemic has had a profound impact on the world, with devastating effects on public health and the global economy. As countries continue to grapple with the ongoing pandemic, it has become increasingly clear that effective and sustainable control measures are crucial in spreading of the virus. Mathematical modeling has played a critical role in understanding the dynamics of the COVID-19 pandemic and in predicting the potential impact of different control strategies. One of the key challenges in developing such models is the incorporation of complex factors that influence the transmission and the control of the disease, such as community awareness and immunity loss. Since the disease began to evolve in early 2020, the scientific community has proposed a plethora of mathematical models. James et al., in their review article [11], have eloquently illustrated the use of mathematical models in combating the diseases while also presenting a lesson for COVID-19 by highlighting some of their limitations and misapplications. Mandal et al. [23] initiated the COVID-19 models in India, and their model was a compartmental model that focused on two main concerns:

* **Corresponding author: Prashant K. Srivastava**, Department of Mathematics, Indian Institute of Technology Patna, Bihta – 801103, Patna, Bihar, India, e-mail: pksri@iitp.ac.in
Sonu Lamba: Department of Mathematics, Indian Institute of Technology Patna, Bihta – 801103, Patna, Bihar, India

the effectiveness of airport screening measures and the best approach to mitigate the spread of the disease once it had reached major cities in India. Subsequently, numerous mathematical models emerged to illustrate the intricate dynamics and projections of the spread of the disease within the country [33]. One such model was presented by Sardar et al. [31], which proposed a novel mathematical model to suggest an effective lockdown strategy.

Several recent studies have employed mathematical modeling techniques to gain insights into various aspects of COVID-19. A recent study by Khan and Abdon [13] centred on the newly emerged Omicron variant and utilized mathematical modeling and analysis to comprehend its transmission dynamics in South Africa. By utilizing the real data from the early stages of the Omicron variant's emergence, the authors estimated parameters to validate their findings accurately. The study's outcomes provided insights into the potential impact of the Omicron variant on disease spread and control strategies. Another study by Kifle and Obsu [14] investigated the transmission dynamics of COVID-19 in Ethiopia using mathematical modeling approaches. The research provided valuable insights into the dynamics of the disease and the effectiveness of different intervention strategies in the Ethiopian context. Their simulation results suggested that controlling the spread of COVID-19 needs reducing contacts among infected individuals and increasing quarantine for those exposed. In the realm of sentiment analysis, a novel approach utilizing a social media-based COVID-19 sentiment classification model was proposed by Arbane et al. [2]. Their model utilizes a bi-directional long short term memory architecture and demonstrates promising results in classifying COVID-19 related sentiments, and the results can be useful in studying impact of negative comments and help counter negative COVID-19 comments and reduce their impact on community awareness. Furthermore, forecasting COVID-19 cases and analyzing the effects of government interventions have been an active area of research. The recent study by Li et al. [20] have employed a novel mathematical model to forecast the spread of the virus and evaluate the impact of different interventions on disease transmission. Contact tracing, a crucial aspect of COVID-19 control, has also been extensively studied in the literature. A very recent systematic review by Juneau et al. [12] highlighted the effectiveness of contact tracing methods and provided insights into strategies for improving its efficacy. Collectively, all these studies have contributed to our understanding of COVID-19 dynamics, control strategies, sentiment analysis, forecasting, contact tracing, isolation guidelines, and healthcare planning in the face of the ongoing pandemic.

Multiple studies have utilized actual data from heavily impacted countries to analyze various aspects of the outbreak and evaluate the effectiveness of interventions such as lockdowns to contain the spread [3,16,27–29]. Numerous studies have investigated the impact of media or information on disease progression. For example, Zhou et al. [39] conducted one of the earliest studies that involved media reporting. The results suggested that, in addition to improving medical interventions, media coverage can serve as an effective strategy to mitigate disease spread during the initial stages of an outbreak. Likewise, several other studies [5,7,15,25,35] have examined the impact of media campaigns on disease transmission. Some of these studies included an additional compartment in their models, while others accounted for a decrease in the force of infection by considering a reduction parameter. However, there have been only a few studies that have investigated community awareness during the susceptibility stage. One such study is the model developed by Ghosh and Martcheva [9], which incorporated the impact of awareness by considering two compartments at the susceptibility level. In light of this model, we propose introducing immunity loss for the recovered population and implementing two time-dependent controls for the exposed, un-notified, and notified infectives. Incorporating waning immunity into COVID models was initially explored by Batistela et al. [4]. However, there have been relatively few studies that have included immunity loss in modeling. Notably, Ghosh and Ghosh [10] recently published a study that highlights the role of waning immunity in disease dynamics. Although their publication took a long time, the study was conducted in 2020 during the initial stages of COVID in Italy, India, and Victoria, but it remains a critical contribution to the field. In this study, the authors extended the basic susceptible-exposed-infectious-recovered (SEIR) model to explore various scenarios, including the impact of nonpharmaceutical and pharmaceutical interventions. They also accounted for the possibility of acquired immunity diminishing over time and the potential for reinfection. Another recent study conducted by Srivastava et al. [32] analyzed the influence of information and treatment saturation on an

susceptible-infectious-recovered-infectious model. In addition, the authors quantified the potential impact of optimal controls and identified the optimal strategy based on cost analysis.

The literature mentioned earlier makes it evident that the COVID-19 pandemic has highlighted the need for comprehensive and effective strategies to control disease transmission. Existing transmission models often overlook the crucial role of community awareness in shaping the susceptibility of individuals to the virus. However, it is widely recognized that individuals who are aware of the risks associated with COVID-19 are more likely to adopt preventive measures and modify their behaviour accordingly. In contrast, individuals who lack awareness may engage in casual behaviour, increasing their vulnerability to infection and contributing to the spread of the virus. This gap calls for a novel approach that explicitly incorporates community awareness into the modeling framework. By formulating separate compartments for unaware and aware susceptible populations, we can capture the heterogeneity in behaviours and susceptibility and provide a more realistic understanding of the dynamics of COVID-19 transmission. The model under consideration in this study aims to bridge this gap by integrating community awareness at the susceptibility level, allowing for a more comprehensive analysis of the effectiveness and cost-effectiveness of control interventions. By considering the impact of awareness on susceptibility, our model offers valuable insights into the complex interplay between behaviour, awareness, and disease transmission, ultimately informing the development of targeted strategies to mitigate the spread of COVID-19. This model allows us to better capture the optimal utilization of intervention strategies, which is the main component we are exploring here through cost-effective optimal control analysis.

In this study, we emphasize the importance of developing appropriate model to evaluate the effectiveness of control measures against disease outbreaks, and we present cost-effective optimal control analysis of a COVID-19 transmission model incorporating community awareness and loss of immunity. Specifically, in addition to the consideration of waning immunity in the model, we establish an optimal control problem (OCP) that includes two time-dependent controls. We introduce “home quarantine” as a control measure to aid the natural recovery of un-notified infectives and exposed individuals. We also incorporate “additional treatment effort” as a control measure for notified infectives who are at a higher risk of transmitting the disease. To determine the most cost-effective combination of control interventions, we use the Pontryagin’s minimization principle (PMP) and forward–backward sweep method (FBSM) to solve the OCP. Our results are further validated through numerical simulation.

The documentation of this article goes like this: the next section presents the mathematical model under consideration, with its positivity and boundedness and computation of reproduction number and investigation of impact of controls, awareness, and waning immunity on it. The subsequent section provides the establishment of the optimality system including formulation of cost functional, existence, and characterization of optimal control functions. After which, we discuss the results obtained from numerical simulations, and finally, the article is concluded in the last section.

2 Mathematical model with controls

This section presents the formulation of a deterministic compartmental S2EI2RS model for COVID-19 transmission with application of controls, incorporating community awareness and immunity loss. This model is primarily based on an SEIR model given by Ghosh and Martcheva [9], where the effects of prosocial awareness on the spread of COVID-19 disease specifically in the context of India and Colombia have been studied. In S2EI2RS model, “*S*2” represents that there are two compartments of susceptible population, (1) S_{ua} - unaware susceptibles and (2) S_a – aware susceptibles; “*E*” denotes the exposed population class; “*I*2” stands for two infectious classes; I_{un} is the un-notified infectives; I_n represents the notified infectives; “*R*” denotes removed individuals (individuals either recovered or do not transmit the disease); and “*S*” at the end represents that people are losing their immunity and moving back to the aware susceptible class S_a (as the immunity waning population is now aware about the disease). Therefore, the total population at a time $t > 0$, $N(t)$ is divided into six mutually separate population compartments, *viz*., $S_{ua}(t)$, $S_a(t)$, $E(t)$, $I_{un}(t)$, $I_n(t)$, and $R(t)$.

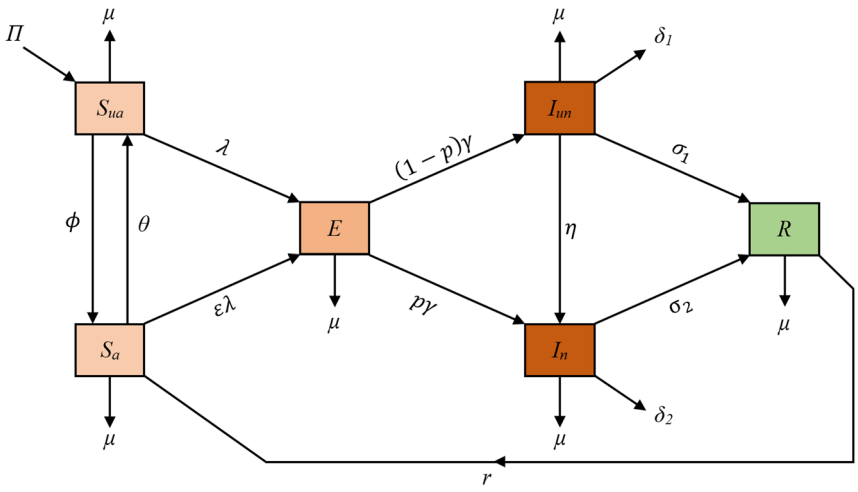

Figure 1: Compartmental model diagram depicting population flow rates through various classes.

A net susceptibility recruitment rate Λ is considered as the mathematical model considers a behavioural response among persons susceptible to the disease, and the unaware susceptibles become aware via communal connections with the aware people. The rate function for this community awareness phenomenon is considered as $\phi = \frac{\alpha S_a}{N}$, where α is the awareness parameter; the population flow from the unaware susceptible class to the aware susceptible class will occur through this rate. The awareness susceptibility may be reduced due to dissemination of any false or unauthentic information, and this transfer is represented by the rate θ. People in both the susceptible classes become exposed to the infection through contact with infectives. Notified infectives are assumed to have reduced transmission due to their access to special care and avoidance of standard mixing, whereas un-notified infectives transmit the disease with the general force of infection. Therefore, the force of infection is considered as $\lambda = \frac{\beta(I_{un} + \nu I_n)}{N}$, where ν is the modification parameter for the notified infectives. As the aware susceptibles will further exercise precautions while having communal meetings with the infectives, therefore, the force of infection for them is considered to be reduced by factor ε. Further, p proportion from the exposed class moves to the notified infectives class, while the rest $(1 - p)$ proportion goes to the un-notified class with a rate of γ. Due to screening or diagnosis, un-notified infectives move to notified class with η rate. The un-notified and notified infectives gain natural immunity with σ_1 and σ_2 rates, respectively. We also consider that the immunity gain is not permanent; therefore, people from recovered class are moving back to the aware susceptible class with a rate r. Note that μ is the natural death rate, which is considered in all population classes; δ_1 and δ_2 are additional disease-induced death rates for un-notified and notified infective classes, respectively. In addition, we consider two time-dependent controls:

(1) **Home quarantine** $u_1(t)$ implemented to exposed and un-notified infective classes, which includes additional immunity-gain effort by not mingling with the notified infectives and exercising self-precautionary measures.
(2) **Additional treatment effort** $u_2(t)$ implemented to notified infective class. These treatment efforts include providing medication, hospitalization, and necessary paramedical facilities to the infectives timely.

Under these assumptions, the population flow and dynamics of the model are described in Figure 1 and represented by the following set of nonlinear differential equations:

$$
\begin{aligned}
\frac{dS_{ua}}{dt} &= \Lambda - (\lambda + \phi + \mu)S_{ua} + \theta S_a \\
\frac{dS_a}{dt} &= \phi S_{ua} - \varepsilon\lambda S_a - (\mu + \theta)S_a + rR \\
\frac{dE}{dt} &= \lambda(S_{ua} + \varepsilon S_a) - (\gamma + \mu + u_1(t))E \\
\frac{dI_{un}}{dt} &= (1 - p)\gamma E - (\eta + \mu + \sigma_1 + \delta_1 + u_1(t))I_{un} \\
\frac{dI_n}{dt} &= p\gamma E + \eta I_{un} - (\mu + \sigma_2 + \delta_2 + u_2(t))I_n \\
\frac{dR}{dt} &= (\sigma_1 + u_1(t))I_{un} + (\sigma_2 + u_2(t))I_n + u_1(t)E - (\mu + r)R,
\end{aligned}
\tag{1}
$$

where $\phi = \frac{\alpha S_a}{N}$ is the community awareness rate function and $\lambda = \frac{\beta(I_{un} + \nu I_n)}{N}$ is the force of infection, with the initial conditions $(S_{ua}(0), S_a(0), E(0), I_{un}(0), I_n(0), R(0))^T \in \mathbb{R}^6_+$ and $u_1(t),\ u_2(t) \in A_U$, where $A_U = \{(u_1, u_2)$: u_1, u_2 measurable, $0 \le u_1, u_2 \le 1, t \in [0, t_f]\}$ is the admissible set of controls. From now on, for the sake of convenience, we may occasionally refer to $u_1(t)$ and $u_2(t)$ as u_1 and u_2, respectively. All the parameters under consideration, their description, and values are given in Table 1.

2.1 Positive invariability and boundedness of the model

This subsection provides the positive invariability and boundedness of the proposed model system. By showing that the model remains within biologically meaningful ranges, and we can ensure that it is a viable tool for studying the behaviour of the biological system of interest. Following the approach given in refs [18,32], we prove the positive invariability and boundedness of the system.

Theorem 2.1. *Assuming that all parameters and controls are nonnegative, the model system* (1) *exhibits positively invariable and bounded solutions within the region*

Table 1: Description and values of the parameters used in the model; values are either assumed suitably or taken within 95% confidence interval of estimations done in ref. [9] or sourced from other reference mentioned

Parameter	Description	Value/Range	Source
Λ	Susceptibility recruitment rate	$\mu \times N$	*
α	Awareness parameter	0.0960 (0.0100–0.0980)	[9,26]
θ	Transfer rate ($S_a \to S_{ua}$)	0.02	[30]
β	Transmission rate	0.6330 (0.5011–0.6509)	[9]
ν	Modification parameter for I_n	0.2131 (0.1231–0.2309)	[9]
ε	Reduction factor for S_a	0.1950 (0.0119–0.2430)	[9]
γ	Incubation period ($1/\gamma$)	0.2	[21]
p	Proportion of I_n	0.2	[38]
η	Transfer rate ($I_{un} \to I_a$)	0.9010 (0.5685–0.9940)	[9]
μ	Natural death rate (in all classes)	0.0000389	*
δ_1	Disease related death rate in I_{un}	0.0631 (0.0012–0.1503)	[9]
δ_2	Disease related death rate in I_n	0.0019 (0.0005–0.0028)	[9]
σ_1	Rate of recovery ($I_{un} \to R$)	0.17	[34]
σ_2	Rate of recovery ($I_n \to R$)	0.072	[22]
r	Rate of waning immunity	Varied (0.2–0.0002)	Assumed
N	Total population (India)	1.38×10^9	*

* indicates that N and μ are demographic as per ref. [9].

$$\Gamma = \left\{(S_{ua}, S_a, E, I_{un}, I_n, R) \in \mathbb{R}^6_+ : 0 \le S_{ua}, S_a, E, I_{un}, I_n, R \le \frac{\Lambda}{\mu}\right\}.$$

Proof. From the model system (1), considering that a particular state vanishes at a time t_0 before the other states become zero, we deduce the following at time t_0

$$\left.\frac{dS_{ua}}{dt}\right|_{S_{ua}=0} = \Lambda + \theta S_a \ge 0, \quad \left.\frac{dS_a}{dt}\right|_{S_a=0} = rR \ge 0, \quad \left.\frac{dE}{dt}\right|_{E=0} = \lambda(S_{ua} + \varepsilon S_a) \ge 0,$$
$$\left.\frac{dI_{un}}{dt}\right|_{I_{un}=0} = (1-p)\gamma E \ge 0, \quad \left.\frac{dI_n}{dt}\right|_{I_n=0} = p\gamma E + \eta I_{un} \ge 0, \quad \left.\frac{dR}{dt}\right|_{R=0} = (\sigma_1 + u_1(t))I_{un} + (\sigma_2 + u_2(t))I_n + u_1(t)E \ge 0.$$

This indicates that each particular state is a nondecreasing time-dependent function; therefore, all state variables are nonnegative if we choose nonnegative initial conditions. Hence, $\mathbb{R}^6_+$ is an invariant set for the system or $(S_{ua}, S_a, E, I_{un}, I_n, R) \in \mathbb{R}^6_+$. Now, to prove the boundedness, we note that the total population $N = S_{ua} + S_a + E + I_{un} + I_n + R$. On differentiating, we obtain $\frac{dN}{dt} = \Lambda - \mu N - \delta_1 I_{un} - \delta_2 I_n \le \Lambda - \mu N$, and by using the comparison theorem [18], we obtain $N(t)$ at a time t

$$N(t) \le \frac{\Lambda}{\mu} - \left(\frac{\Lambda}{\mu} - N(0)\right)e^{-\mu t}. \tag{2}$$

If $N(0) \le \frac{\Lambda}{\mu}$, then $N(t) \le \frac{\Lambda}{\mu}$, and if $N(0) > \frac{\Lambda}{\mu}$, then $\lim_{t\to\infty} N(t) = \frac{\Lambda}{\mu}$. It means that all solutions with initial conditions in Γ remain in Γ for all future times. Hence, the set Γ is a positively invariable attractor for the solutions of the model system (1) in $\mathbb{R}^6_+$. □

Figure 2 displays the disease prevalence in the absence of any control measures, that is, when $u_1 = 0 = u_2$. The initial population densities used in the simulation are indicated in the figure caption.

2.2 Reproductive threshold with respect to controls

The system (1) exhibits an infection-free equilibrium, denoted and given by

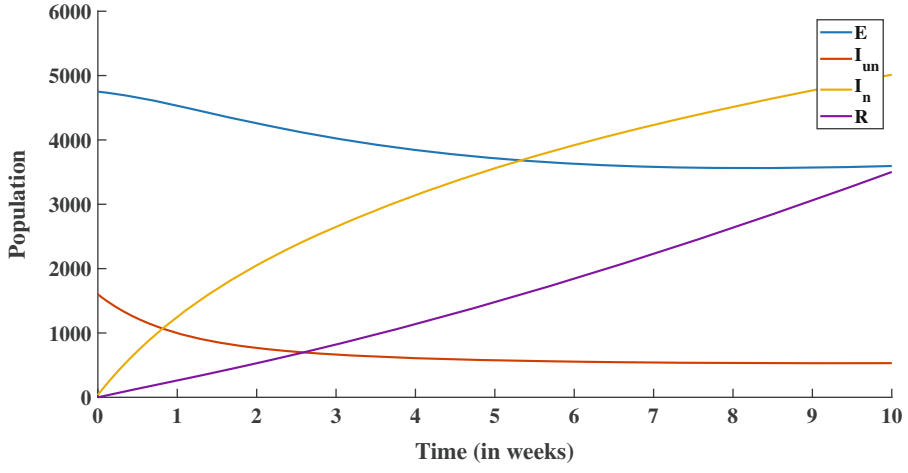

Figure 2: Disease prevalence when no control is applied to the model, i.e., $u_1 = 0$ and $u_2 = 0$, with $S_{ua}(0) = 0.9 \times N$, $S_a(0) = 10{,}000$, $E(0) = 4{,}750$, $I_{un}(0) = 1{,}600$, $I_n(0) = 38$, and $R(0) = 0$ as initial population densities.

$$E_0 = (S_{ua}, S_a, 0, 0, 0, 0) = \left(\frac{\Lambda(\mu + \theta)}{\mu\alpha}, \frac{\Lambda(\alpha - (\mu + \theta))}{\mu\alpha}, 0, 0, 0, 0\right),$$

provided, $\alpha - (\mu + \theta) > 0$ or $\frac{\alpha}{\mu + \theta} > 1$, i.e. awareness parameter related to the aware susceptible individuals must be greater than the combined value of awareness reduction parameter and natural death rate. Now, by using the next-generation matrix approach [36], we obtain the reproductive threshold or the basic reproduction number, which is the average number of secondary infections induced by one infective individual in a fully susceptible population during the infectious period. We represent $X = (E, I_{un}, I_n)^T$ as a column vector of the infective state variable or compartments and obtain the following equation:

$$\frac{\mathrm{d}X}{\mathrm{d}t} = \frac{\mathrm{d}}{\mathrm{d}t}\begin{pmatrix} E \\ I_{un} \\ I_n \end{pmatrix} = \mathcal{F} - \mathcal{V},$$

where $\mathcal{F}$ and $\mathcal{V}$ are the column vectors of new infection terms and transition terms, respectively, written out from the infective state equations as follows:

$$\mathcal{F} = \begin{pmatrix} \frac{\beta(I_{un} + \nu I_n)}{N}(S_{ua} + \varepsilon S_a) \\ 0 \\ 0 \end{pmatrix}, \quad \mathcal{V} = \begin{pmatrix} (\gamma + \mu + u_1)E \\ -(1 - p)\gamma E + (\eta + \mu + \sigma_1 + \delta_1 + u_1)I_{un} \\ -p\gamma E - \eta I_{un} + (\mu + \sigma_2 + \delta_2 + u_2)I_n \end{pmatrix}.$$

By finding Jacobian of these column vectors, we obtain matrices $F = \mathcal{J}(\mathcal{F})|_{E_0}$ and $V = \mathcal{J}(\mathcal{V})|_{E_0}$ as follows:

$$F = \mathcal{J}(\mathcal{F})|_{E_0} = \begin{pmatrix} 0 & \beta k_4 & \nu\beta k_4 \\ 0 & 0 & 0 \\ 0 & 0 & 0 \end{pmatrix}, \quad V = \mathcal{J}(\mathcal{V})|_{E_0} = \begin{pmatrix} k_1 & 0 & 0 \\ -(1 - p)\gamma & k_2 & 0 \\ -p\gamma & -\eta & k_3 \end{pmatrix},$$

where $k_1 = \gamma + \mu + u_1$, $k_2 = \eta + \mu + \sigma_1 + \delta_1 + u_1$, $k_3 = \mu + \sigma_2 + \delta_2 + u_2$, and $k_4 = \frac{1}{\alpha}[(\theta + \mu) + \varepsilon(\alpha - (\theta + \mu))]$.

$$\Rightarrow FV^{-1} = \begin{pmatrix} 0 & \beta k_4 & \nu\beta k_4 \\ 0 & 0 & 0 \\ 0 & 0 & 0 \end{pmatrix} \begin{pmatrix} \frac{1}{k_1} & 0 & 0 \\ \frac{(1 - p)\gamma}{k_1 k_2} & \frac{1}{k_2} & 0 \\ \frac{(1 - p)\gamma\eta + p\gamma k_2}{k_1 k_2 k_3} & \frac{\eta}{k_2 k_3} & \frac{1}{k_3} \end{pmatrix},$$

$$= \begin{pmatrix} \frac{\beta k_4(1 - p)\gamma}{k_1 k_2} + \frac{\nu\beta k_4(1 - p)\gamma\eta + \nu\beta k_4 p\gamma k_2}{k_1 k_2 k_3} & \frac{\beta k_4}{k_2} + \frac{\nu\beta k_4\eta}{k_2 k_3} & \frac{\nu\beta k_4}{k_3} \\ 0 & 0 & 0 \\ 0 & 0 & 0 \end{pmatrix}.$$

The basic reproduction number ($\mathcal{R}_0$) is given by the dominated eigenvalue of the next generation matrix FV^{-1}, i.e., $\rho(FV^{-1}) = \mathcal{R}_0$; therefore, we have

$$\mathcal{R}_0 = \frac{\beta k_4 \gamma}{k_1 k_2 k_3}[(1 - p)(\nu\eta + k_3) + \nu p k_2]. \tag{3}$$

We explore the effects of the controls on the reproductive threshold and determined using the next-generation matrix method given earlier (3). We visualize it by plotting a surface plot of R_0 against the constant values of controls u_1 and u_2 in the range $[0, 1] \times [0, 1]$. Figure 3 indicates that the full efforts of applying both controls ($u_1 = 1 = u_2$) simultaneously achieve the lowest value of R_0 (0.0918) compared to other scenarios, suggesting that this approach is most effective in achieving a disease-free environment. However, it may not be cost-effective for which we discuss OCP in the next section.

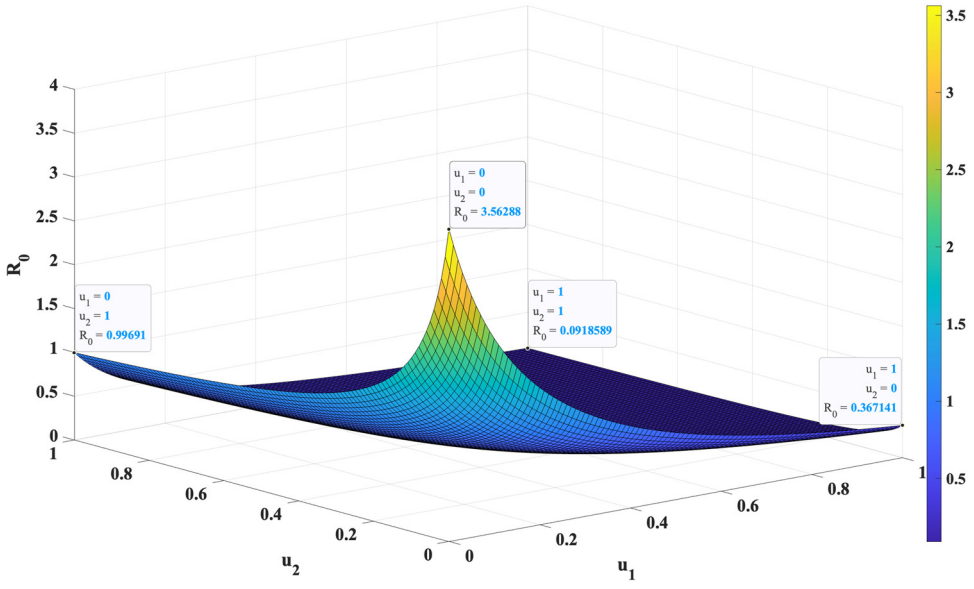

Figure 3: Surface plot depicting the variation of $\mathcal{R}_0$ with respect to controls u_1 and u_2, taking parameters values/in the range mentioned in Table 1.

2.3 Effect of community awareness and warning immunity

In this subsection, we examine the effects of increasing the awareness parameter on the reproduction number in the absence of any control measures, i.e., $u_1 = 0 = u_2$. Furthermore, we investigate the impact of the loss of immunity on the recovery rate. By focusing on these two key factors, we aim to gain a deeper understanding of the dynamics of disease transmission and recovery within a community. Through our analysis, we explore the implications of heightened community awareness and the consequences of waning immunity on the overall control and management of the disease.

From Figure 4 it is evident that increment in awareness parameter α cause a decrement in reproduction number R_0, which means that community awareness plays a crucial role in reducing disease prevalence. These results emphasize the importance of implementing robust awareness campaigns and education initiatives to enhance public understanding and promote proactive measures against the disease. The red line in Figure 4 represents $R_0 = 1$ threshold. Maintaining a sufficiently high level of community awareness has the potential to drive the reproduction number R_0 below unity (i.e., $R_0 < 1$). This indicates that the number of secondary infections would not exceed one, signifying a shift towards disease eradication. By achieving such a state, the spread of the disease can be effectively controlled and ultimately halted. Thus, prioritizing and sustaining community awareness initiatives become crucial in striving for the eradication of the disease.

Immunity loss can have a significant effect on number of recoveries when no control is applied. The Figure 5 clearly demonstrates that as the rate of waning immunity (r) increases, there is a significant depletion observed in the number of individuals who recover from the disease. The red curve is when $r = 0.2$, that is, at the high rate of immunity loss, the number of recovered individuals is low. However, when $r = 0.0002$, the number recoveries are high. There is a huge difference in number of recovered individuals at the end of the time duration, in both cases.

3 Establishment of optimality system

This section describes formulation of cost-functional and establishment of optimality system corresponding to the model (1). We first construct a cost functional that is to be optimized and then prove the existence and characterization of optimal controls to write the optimality system.

3.1 Formulation of cost functional

For each bounded control variable in A_U, the system (1) is invariant in $\mathbb{R}^6_+$ and bounded in the region Γ. The *objective cost functional* with respect to system (1) is a weighted combination of two cost components:

Cost related to disease prevalence: The cost incurred due to disease prevalence refers to the economic burden that arises from the presence of a particular disease in a population.

$$\int_0^{t_f} (W_1E(t) + W_2I_{un}(t) + W_3I_n(t))\mathrm{d}t.$$

The cost component related to disease prevalence includes various factors, such as, direct medical costs, indirect costs (economic impact of the disease on the productivity of the affected individuals and the society as a whole, loss of workdays, reduced productivity, and disability), and intangible costs (nonmonetary costs that are difficult to quantify, such as pain, suffering, and reduced quality of life). As these factors are directly dependent on the density of infectives (exposed, un-notified, and notified), we take this cost component directly proportional to different infectives population balanced with appropriate weights.

Cost related to control implementation: This refers to the expenses associated with implementing the controls u_1 and u_2.

$$\int_0^{t_f} \frac{1}{2}(Z_1u_1^2(t) + Z_2u_2^2(t))\mathrm{d}t.$$

The nonlinear nature of this cost component arises from the fact that implementing control interventions becomes increasingly challenging and resource intensive as the related efforts increase.

Therefore, the total cost that to be minimized is given by

$$\mathcal{J}(u_1(t), u_2(t)) = \int_0^{t_f} \left[W_1E(t) + W_2I_{un}(t) + W_3I_n(t) + \frac{1}{2}(Z_1u_1^2(t) + Z_2u_2^2(t)) \right] \mathrm{d}t, \tag{4}$$

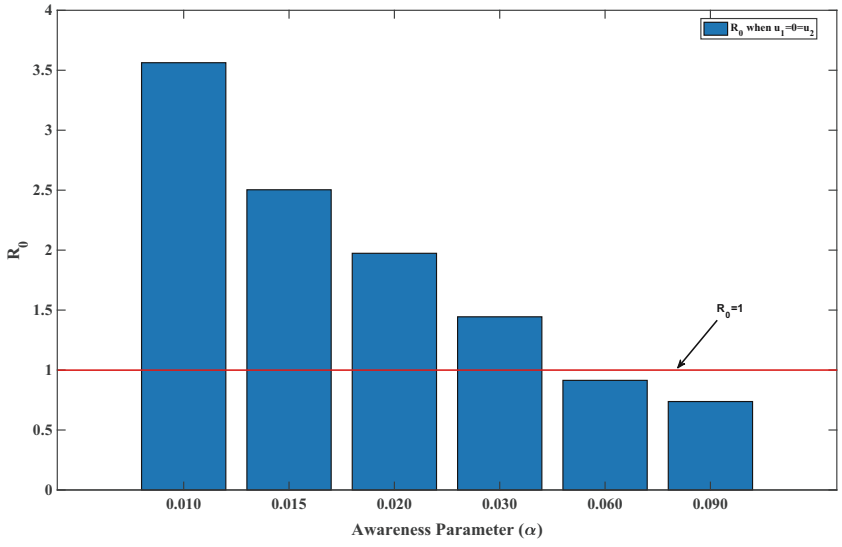

Figure 4: Bar plot depicting variation of reproduction number R_0 with respect to awareness parameter α.

where W_1, W_2, W_3, Z_1, and Z_2 are the positive weight constants, chosen to balance the costs as per the size and significance of the respective components of the cost functional. Our main objective is to control disease transmission while keeping costs to a minimum, that is, we need to determine the doublet (u_1^*, u_2^*) that satisfies

$$\mathcal{J}(u_1^*, u_2^*) = \min\{\mathcal{J}(u_1, u_2) | u_1, u_2 \in A_U\}. \tag{5}$$

3.2 Optimal control functions: existence and characterization

In this subsection, we show that the optimal control functions (that minimize the cost functional in a finite time) exists and are well posed or characterized. By using the approaches given in refs [8,17,32], we state and prove the following sufficient and necessary conditions.

Theorem 3.1. *There exist a doublet* (u_1^*, u_2^*) *in* A_U *that satisfies* (5) *if the following conditions hold*

(1) *With* $(u_1, u_2) \in A_U$, *the solution set of system* (1) *is nonempty*.

(2) *The state system* (1) *can be expressed as a linear function of control variables whose coefficients vary based on time and state variables. In addition,* A_U *is both closed and convex*.

(3) *The integrand of* (4), i.e., $\mathcal{L} = W_1E(t) + W_2I_{un}(t) + W_3I_n(t) + \frac{1}{2}(Z_1u_1^2(t) + Z_2u_2^2(t))$ *is convex in* A_U *and* $\mathcal{L} \geq f(u_1, u_2)$, *where* f *is continuous and* $\frac{f(u_1,u_2)}{|(u_1,u_2)|} \to \infty$ *as* $|(u_1, u_2)| \to \infty$.

Proof. The solutions of system (1) are both positively invariant and bounded within Γ, as demonstrated in Theorem 2.1. Also, the Lipschitz condition is satisfied by the right-hand side of all equations in the model system with respect to state variables. As a result, the first condition is guaranteed by utilizing the Picard-Lindelof theorem [6].

The admissible control set A_U is closed and convex by definition; the system (1) is linear in control variables; therefore, the second condition is also satisfied. Further, the integrand $\mathcal{L} = W_1E(t) + W_2I_{un}(t) + W_3I_n(t) + \frac{1}{2}(Z_1u_1^2(t) + Z_2u_2^2(t))$ is convex due to its quadratic nature, and it can be easily shown [32] by definition. Now, let $Z = \min(Z_1, Z_2) > 0$ and $f(u_1, u_2) = Z(u_1^2 + u_2^2)$, then $\mathcal{L} \geq f(u_1, u_2)$, and clearly, f is continuous and $\frac{f(u_1,u_2)}{|(u_1,u_2)|} \to \infty$ as $|(u_1, u_2)| \to \infty$; so, the last condition is also fulfilled. Thus, the proof. □

Now, to make use of the PMP [19], we formulate the Hamiltonian $H(\mathbf{x}, \mathbf{u}, \lambda)$, which is a sum of the integrand $\mathcal{L}(t, \mathbf{x}, \mathbf{u})$ and $\sum_{i=1}^{5}\lambda_i\frac{dx_i}{dt}$, given by

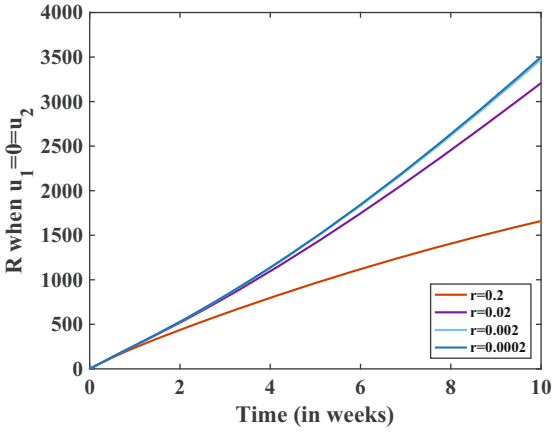

Figure 5: Effect of immunity loss on recoveries from disease in absence of any control intervention.

$$H(\mathbf{x}, \mathbf{u}, \lambda) = \mathcal{L}(t, \mathbf{x}, \mathbf{u}) + \lambda_1 \frac{\mathrm{d}S_{ua}(t)}{\mathrm{d}t} + \lambda_2 \frac{\mathrm{d}S_a(t)}{\mathrm{d}t} + \lambda_3 \frac{\mathrm{d}E(t)}{\mathrm{d}t} + \lambda_4 \frac{\mathrm{d}I_{un}(t)}{\mathrm{d}t} + \lambda_5 \frac{\mathrm{d}I_n(t)}{\mathrm{d}t} + \lambda_6 \frac{\mathrm{d}R(t)}{\mathrm{d}t},$$

where $\mathbf{x}$ and $\mathbf{u}$ represent the vectors of state and control variables, respectively; $\lambda = (\lambda_1, \lambda_2, \lambda_3, \lambda_4, \lambda_5, \lambda_6) \in \mathbb{R}^6$ is known as adjoint vector, elements of which satisfies

$$\frac{\mathrm{d}\lambda_1(t)}{\mathrm{d}t} = -\frac{\partial H}{\partial S_{ua}}, \frac{\mathrm{d}\lambda_2(t)}{\mathrm{d}t} = -\frac{\partial H}{\partial S_a}, \frac{\mathrm{d}\lambda_3(t)}{\mathrm{d}t} = -\frac{\partial H}{\partial E}, \frac{\mathrm{d}\lambda_4(t)}{\mathrm{d}t} = -\frac{\partial H}{\partial I_{un}}, \frac{\mathrm{d}\lambda_5(t)}{\mathrm{d}t} = -\frac{\partial H}{\partial I_n}, \text{ and } \frac{\mathrm{d}\lambda_6(t)}{\mathrm{d}t} = -\frac{\partial H}{\partial R}, \tag{6}$$

with transversality conditions $\lambda_1(t_f) = 0$, $\lambda_2(t_f) = 0$, $\lambda_3(t_f) = 0$, $\lambda_4(t_f) = 0$, $\lambda_5(t_f) = 0$, and $\lambda_6(t_f) = 0$.

Theorem 3.2. *Given the existence of an optimal control doublet* (u_1^*, u_2^*) *and the corresponding state variables* $(S_{ua}^*, S_a^*, E, I_{un}^*, I_n^*, R^*)$ *that optimize the objective cost functional* (4)*, there exist* λ_1, λ_2, λ_3, λ_4, λ_5, *and* λ_6, *satisfying the adjoint system* (6) *with transversality conditions, then the doublet of optimal controls can be characterized as follows*:

$$\begin{aligned} u_1^* &= \max\left\{\min\left\{\frac{(\lambda_4 - \lambda_6)I_{un}^* + \lambda_3 E^*}{Z_1}, 1\right\}, 0\right\}, \\ u_2^* &= \max\left\{\min\left\{\frac{(\lambda_5 - \lambda_6)I_n^*}{Z_2}, 1\right\}, 0\right\}. \end{aligned} \tag{7}$$

Proof. As per the approach followed in ref. [32], the optimal doublet (u_1^*, u_2^*) given in (7) is obtained by using the PMP and optimality conditions, $\frac{\partial H}{\partial u_1} = 0$ and $\frac{\partial H}{\partial u_2} = 0$. □

3.3 Optimality system

In this subsection, we summaries the process of formulation described earlier and use the optimal control functions, which are characterized in previous subsection to write the corresponding optimality system. For the OCP with state system (1) and cost functional (4), the *optimality system* with optimized Hamiltonian H^* at $(S_{ua}^*, S_a^*, E^*, I_{un}^*, I_n^*, R^*, u_1^*, u_2^*, \lambda)$ is given by

$$\begin{aligned} \frac{\mathrm{d}S_{ua}^*}{\mathrm{d}t} &= \Lambda - (\lambda^* + \phi^* + \mu)S_{ua}^* + \theta S_a^* \\ \frac{\mathrm{d}S_a^*}{\mathrm{d}t} &= \phi^* S_{ua}^* - \varepsilon\lambda^* S_a^* - (\mu + \theta)S_a^* + rR^* \\ \frac{\mathrm{d}E^*}{\mathrm{d}t} &= \lambda^*(S_{ua}^* + \varepsilon S_a^*) - (\gamma + \mu + u_1^*)E^* \\ \frac{\mathrm{d}I_{un}^*}{\mathrm{d}t} &= (1 - p)\gamma E^* - (\eta + \mu + \sigma_1 + \delta_1 + u_1^*)I_{un}^* \\ \frac{\mathrm{d}I_n^*}{\mathrm{d}t} &= p\gamma E^* + \eta I_{un}^* - (\mu + \sigma_2 + \delta_2 + u_2^*)I_n^* \\ \frac{\mathrm{d}R^*}{\mathrm{d}t} &= (\sigma_1 + u_1^*)I_{un}^* + (\sigma_2 + u_2^*)I_n^* + u_1^* E^* - (\mu + r)R^*, \end{aligned} \tag{8}$$

where $\phi^* = \frac{\alpha S_a^*}{N}$ is the optimal community awareness rate function and $\lambda^* = \frac{\beta(I_{un}^* + \nu I_n^*)}{N}$ is the optimal force of infection, with the initial conditions $(S_{ua}^*(0), S_a^*(0), E^*(0), I_{un}^*(0), I_n^*(0), R^*(0))^T \in \mathbb{R}_+^6$ and $u_1^*(t), u_2^*(t) \in A_U$, and the corresponding *adjoint system* is

$$
\begin{aligned}
\frac{\mathrm{d}\lambda_1(t)}{\mathrm{d}t} &= \lambda^*(\lambda_1 - \lambda_3) + \phi^*(1 - \lambda_2) + \mu\lambda_1 \\
\frac{\mathrm{d}\lambda_2(t)}{\mathrm{d}t} &= \left(\frac{\alpha S_u^*}{N} - \theta\right)\lambda_1 - \left(\frac{\alpha S_u^*}{N} - \varepsilon\lambda^* - \mu - \theta\right)\lambda_2 - \lambda^*\lambda_3 \\
\frac{\mathrm{d}\lambda_3(t)}{\mathrm{d}t} &= -W_1 + (\gamma + \mu + u_1^*)\lambda_3 - (1 - p)\gamma\lambda_4 - p\gamma\lambda_5 - u_1^*\lambda_6 \\
\frac{\mathrm{d}\lambda_4(t)}{\mathrm{d}t} &= -W_2 + \frac{\beta S_u^*}{N}\lambda_1 + \frac{\varepsilon\beta S_a^*}{N}\lambda_2 - \frac{\beta(S_u^* + \varepsilon S_a^*)}{N}\lambda_3 + (\eta + \sigma_1 + \mu + \delta_1 + u_1^*)\lambda_4 - \eta\lambda_5 - (\sigma_1 + u_1^*)\lambda_6 \\
\frac{\mathrm{d}\lambda_5(t)}{\mathrm{d}t} &= -W_3 + \frac{\beta\nu S_u^*}{N}\lambda_1 + \frac{\varepsilon\beta\nu S_a^*}{N}\lambda_2 + \frac{\beta\nu(S_u^* + \varepsilon S_a^*)}{N}\lambda_3 + (\sigma_2 + \mu + \delta_2 + u_2^*)\lambda_5 - (\sigma_2 + u_2^*)\lambda_6 \\
\frac{\mathrm{d}\lambda_6(t)}{\mathrm{d}t} &= -r\lambda_2 + \mu\lambda_6,
\end{aligned}
\tag{9}
$$

with transversality condition $\lambda_i(t_f) = 0\ \forall i$ and the optimal controls are as written in (7). The combination of equations (8)–(7) is termed as the optimality system, which is to be solved and analyzed in the section.

4 Discussion on numerical simulations and results

This section provides an interpretation of the results and discusses the implications of the study. We utilized the FBSM [19] to solve our OCP (optimality system), for the purpose of simulations and discussion of results. The FBSM involves a solution process that starts by solving the state system (8) using the fourth-order Runge-Kutta (RK4) method, with initial conditions, in the forward direction (time). The obtained state solution is then used to solve the adjoint system (9), with transversality conditions, in the backward direction (time) using the RK4 method. The solutions for both the state and adjoint systems are then used to update the control value based on the characterization discussed in (7). This process is repeated iteratively until convergence is achieved for the values of state variables, adjoint variables, and controls [24]. To numerically simulate our OCP, we selected a set of parameter values within the ranges as detailed in Table 1 and initialized the system with initial conditions of $S_{ua}(0) = 0.9 \times N$, $S_a(0) = 10{,}000$, $E(0) = 4{,}750$, $I_{un}(0) = 1{,}600$, $I_n(0) = 38$, and $R(0) = 0$. To ensure effective optimization, we also determined the appropriate weights for the objective cost functional (4). Specifically, we chose $W_1 = 400$, $W_2 = 1{,}000$, $W_3 = 2{,}000$, $Z_1 = 500$, and $Z_2 = 800$. These weights were selected to reflect the different levels of importance and effort required for each control. The controls were implemented over a period of 10 weeks (70 days) to achieve the desired outcomes for our optimization problem. By selecting appropriate parameters and initializing the system with the right initial conditions, we were able to obtain reliable and accurate results for our simulation.

For better discussion and interpretation of optimality and cost-efficacy analysis, we consider three strategies based on implementation of individual control interventions and their combination to be explored numerically:

Strategy A: Single control, $u_1(t)$, i.e., home quarantine implemented on exposed and un-notified infectives.

Strategy B: Single control, $u_2(t)$, i.e., additional treatment effort provided to notified infectives.

Strategy C: Implementation of both controls, $u_1(t)$ and $u_2(t)$, simultaneous.

We now delve into the strategy-wise outcomes of the numerical simulation that is conducted in MATLAB. In addition, at the end, a cost-efficacy analysis is given to identify the most cost-effective strategy among all.

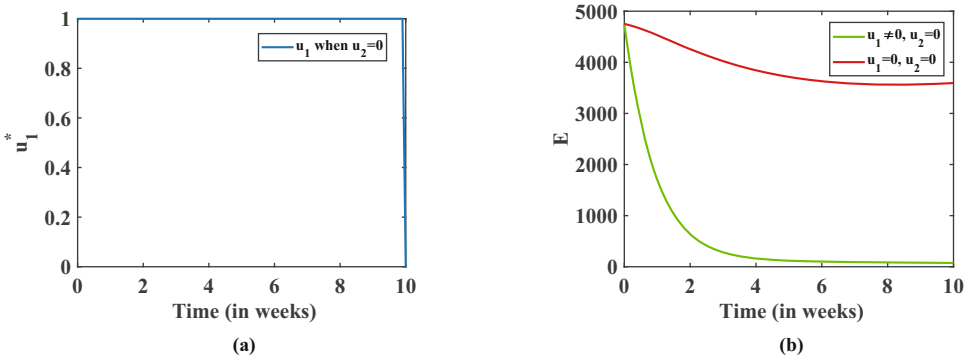

Figure 6: (a) Optimal control path of u_1^* and (b) impact of applying only u_1 on exposed population E.

4.1 Strategy A: only u_1 (home quarantine)

In the first case – strategy A, we have considered an implementation of a single control policy $u_1(t)$, i.e., only home quarantine is employed over the exposed population and un-notified infectives.

In Figure 6(a), we can see that the optimal control profile of u_1^* indicates that if only u_1 is implemented as a single control intervention strategy, it would require full implementation efforts for nearly the entire duration of around 68 days before it can be removed from employment at the end. Furthermore, Figure 6(b) demonstrates the impact of solely implementing u_1 on the exposed population. It is noteworthy that if individuals in the exposed population exercise home quarantine measures, there can be a significant reduction in disease prevalence compared to scenarios where no control intervention is implemented (as depicted by the red curve). This reduction ultimately translates to a lower risk of infection.

Furthermore, Figure 7(a) also depicts that there is a considerable impact of exercising home quarantine by the exposed and un-notified infectives on the I_{un} class of the population. On the other hand, Figure 7(b) shows that even the strategy A is not applicable for the notified infective, it has a significant effect on disease prevalence for I_n class. While there is an increment in number of notified cases for the initial 1 week, but after that, the prevalence goes down significantly.

4.2 Strategy B: only u_2 (additional treatment effort)

Within the scope of Strategy B, our focus is solely on the implementation of additional treatment effort as a single control intervention for notified infectives, given their heightened vulnerability to disease transmission and mortality.

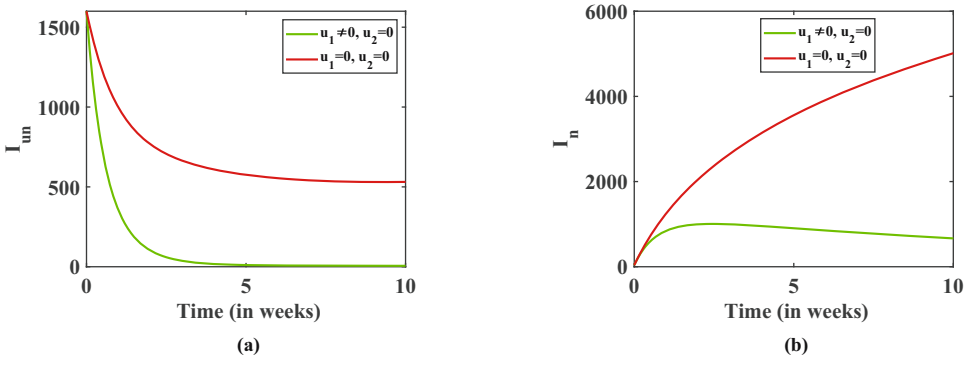

Figure 7: Effect of applying only u_1 on (a) un-notified infectives I_{un} and (b) notified infectives I_n, in comparison with the case when no control is applied ($u_1 = 0 = u_2$).

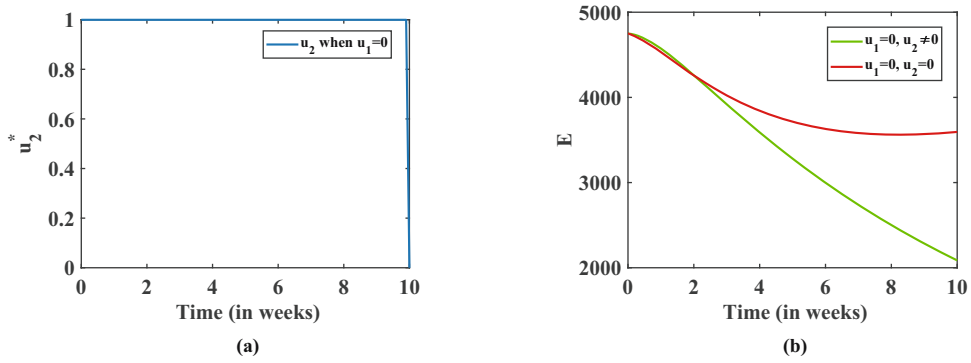

Figure 8: (a) Optimal control path of u_2^* and (b) impact of applying only u_2 on exposed population E.

Giving additional medical aid to the identified infected individuals as a singular measure of control necessitates complete attention (full efforts), as illustrated in Figure 8(a). Since this approach is exclusively intended for the I_n population group, it is apparent that it will have a minimal impact on the disease prevalence of other infectious groups, as demonstrated in Figures 8(b) and 9(a). Nonetheless, it is noted that there is an impact even on the exposed and un-notified population when compared to the disease prevalences in the absence of any control measures.

On the other hand, Figure 9(b) demonstrates that solely implementing u_2 has a significant impact on the identified infected individuals, resulting in even further reduction in the number of cases. This indicates that providing additional treatment effort could be highly beneficial for the identified infected population compared to the scenario where no control measures are implemented. In the subsequent subsection, strategy (B) is compared with the previous strategy (A) to further highlight its effectiveness on the disease prevalence. Additional remarks regarding the effectiveness of this approach are provided in the following subsection on cost-effectiveness analysis (CEA).

4.3 Strategy C: both u_1 and u_2 (home quarantine and additional treatment effort)

Strategy C addresses the scenario where both controls are implemented concurrently, namely, home quarantine and additional treatment effort are applied simultaneously to their respective target population groups.

The optimal profiles depicted in Figure 8(a) and (b) for u_1 and u_2, respectively, indicate that when implementing home quarantine (u_1) as a control measure in conjunction with additional treatment effort ($u_2 \neq 0$), it requires full efforts for a shorter period (approximately 58 days) before it decreases to zero

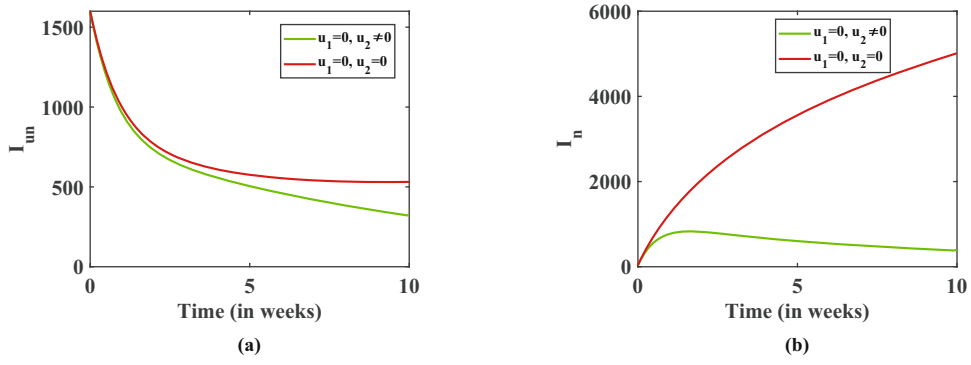

Figure 9: Effect of applying only u_2 on (a) un-notified infectives I_{un} and (b) notified infectives I_n, in comparison with the case when no control is applied ($u_1 = 0 = u_2$).

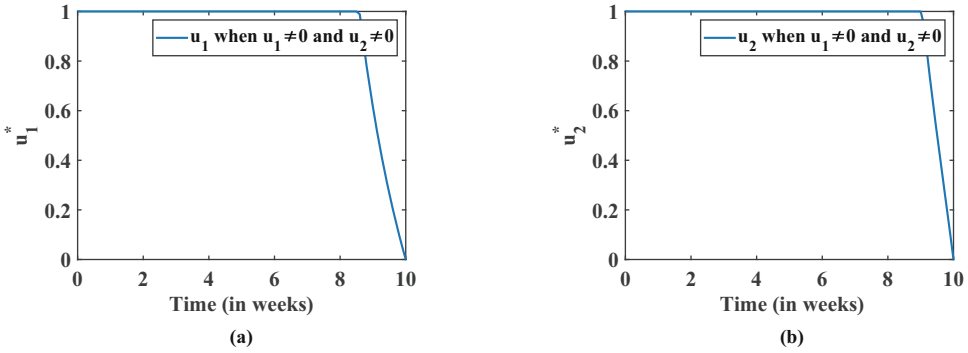

Figure 10: Optimal control paths for (a) home quarantine u_1 and (b) additional treatment effort u_2, when both controls are applied, i.e., $u_1 \neq 0$ and $u_2 \neq 0$.

(removal of control). However, implementing u_2 when $u_1 \neq 0$ requires full attention for 63 days before its reduction (Figure 10(a) and (b)). One possible explanation for this is that the same resources, such as economic and medical resources, are utilized when both controls are employed concurrently. Thus, these resources can be utilized to their fullest potential for a shorter duration.

The combination of both the controls further flatten the disease prevalence curves for all the infective population groups *viz*. exposed E, un-notified infectives I_{un}, and notified infectives I_n, as shown in Figures 11(a) and (b) and 12(a), respectively. It is noted that in the cases, the disease prevalence achieves the subzero level or disease-free state nearly after 5 weeks (almost 35 days, which is half of the control employment time period).

The implementation of both controls concurrently leads to a steeper decline in the number of exposed and un-notified cases. In addition, the prevalence curve for notified infectives also shows a decline in the number of cases, with an initial peak in the first week and a rapid decrease thereafter, ultimately reaching zero just before the fifth week as shown in Figure 12(a). These results demonstrate that the combined use of both controls is highly effective in reducing the number of notified cases.

In Figure 12(b), the impact of Strategy C on the number of individuals in the recovered class is depicted. It is apparent that the simultaneous use of both controls is significantly more effective in increasing the number of recoveries over time. However, there is a saturation point after approximately half of the control measures' duration. Further insights on this behaviour are provided in the following subsection. The effects of applying single controls on the recovered population are not displayed separately in the previous subsection but are discussed in the comparative analysis in the next section.

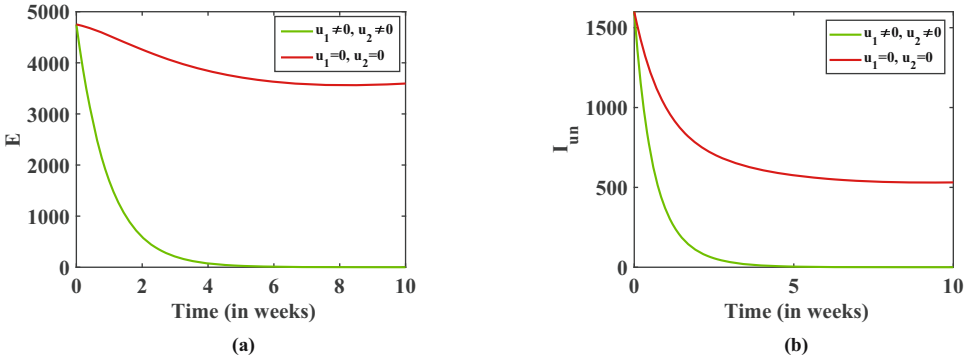

Figure 11: Effect of applying both u_1 and u_2 simultaneously on (a) exposed population E and (b) un-notified infectives I_{un}, in comparison with the case when no control is applied ($u_1 = 0 = u_2$).

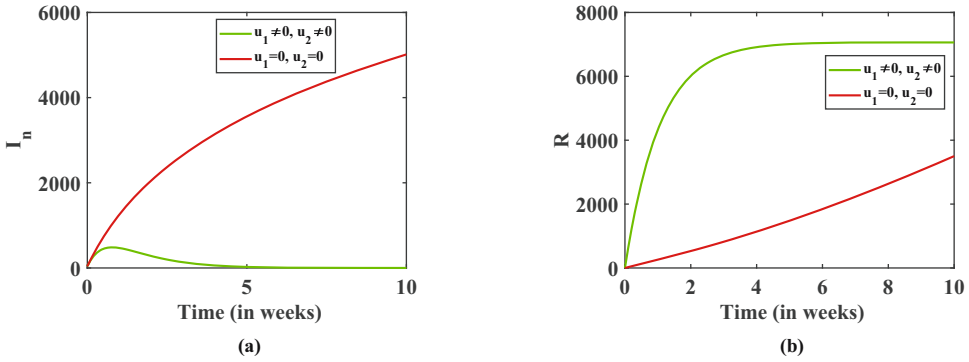

Figure 12: Effect of applying both u_1 and u_2 simultaneously on (a) notified infectives I_n and (b) recovered class of population R, in comparison with the case when no control is applied ($u_1 = 0 = u_2$).

4.4 Comparative study

In this section, we perform a comparative analysis of all three cases discussed earlier: the Strategy A – use of only u_1 as a control, the Strategy B – use of only u_2, and the Strategy C – simultaneous use of both u_1 and u_2, with the case where there are no controls. As depicted in Figure 13(a), implementing the u_1 control when both controls are used requires less effort compared to when only u_1 is used. A similar trend can also be observed in Figure 13(b) for the implementation of the u_2 control. The reduction in the time required for full effort (i.e., controls at the upper bound) is due to the fact that we are utilizing both controls simultaneously, with the same resources and economic conditions, thereby limiting our ability to use them to their full potential for a shorter duration (as discussed in the previous subsection). Figure 14(a) and (b) compares the disease prevalence curves for the exposed and un-notified classes of the population, respectively, across all the scenarios or strategies being evaluated. These figures show that simultaneous application of both the controls is most effective (green curves) in reduced number of exposed and un-notified cases of infections. However, implementation of only u_2 as a control is very less effective (pink dotted curves). A similar pattern is observed for the notified population, but with a more significant reduction in cases. Strategy C is the most effective in terms of disease prevalence, as depicted in Figure 15(a). Figure 15(b) shows the impact of the strategies on the recovered population. It is noteworthy that the case where no control is applied has significantly fewer recoveries compared to the other strategies. Providing only additional treatment (u_2) results in a steep (almost linear) increase in recoveries (pink dotted curve), but the simultaneous implementation of both controls is the most advantageous as the area under the curve (green) is much larger than that of any other case, indicating that the number of recoveries for Strategy C is the highest.

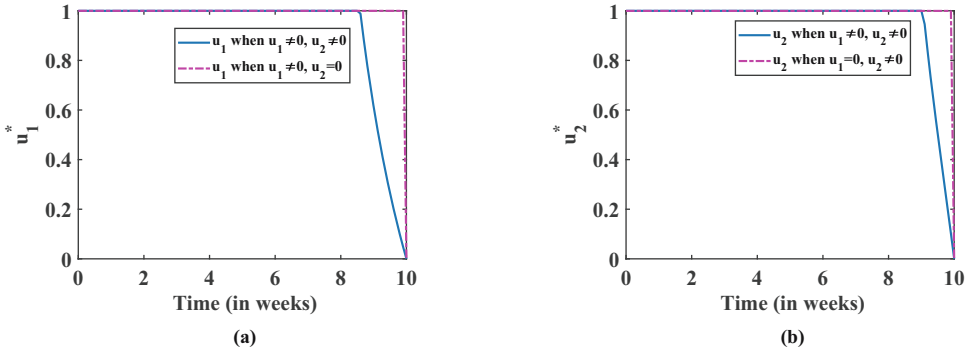

Figure 13: Comparison of optimal control profiles for (a) home quarantine u_1 and (b) additional treatment effort u_2, when only one control is applied (pink dotted curves) and when both controls are applied (blue curves).

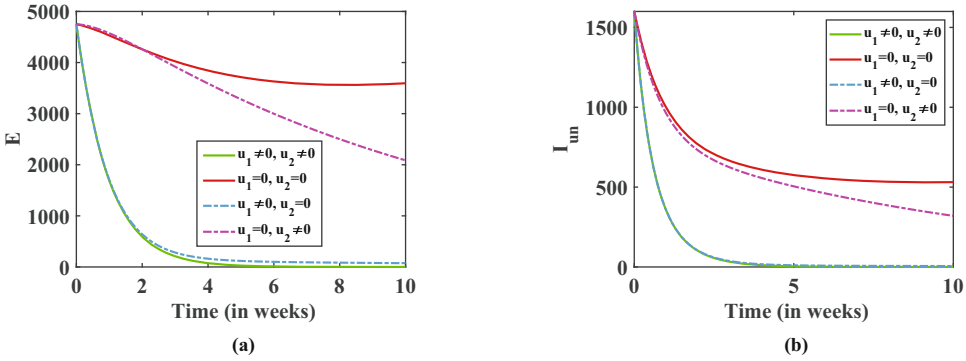

Figure 14: Comparative disease prevalence curves for (a) exposed population E and (b) un-notified infectives I_{un}, in comparison with the case when no control is applied ($u_1 = 0 = u_2$).

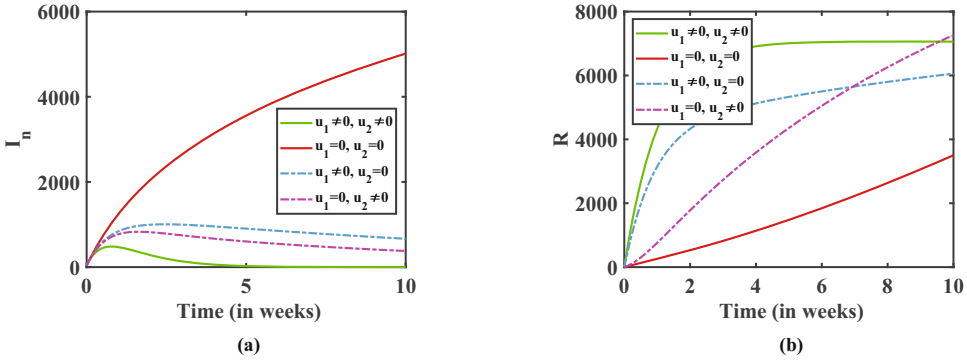

Figure 15: Comparison of optimal control profiles for (a) notified infectives I_n and (b) recovered class of population R, in comparison with the case when no control is applied ($u_1 = 0 = u_2$).

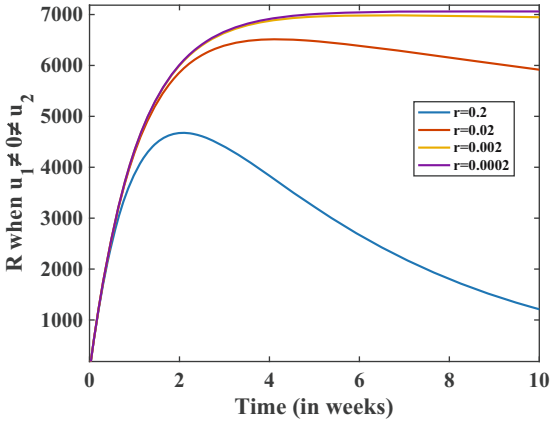

Figure 16: Effect of immunity loss on recoveries from disease when both controls are applied simultaneously.

Figure 16 depicts the impact of immunity loss on number of recovered individuals when both controls are implemented simultaneously, that is, $u_1 \neq 0 \neq u_2$. It can be seen that when immunity loss is high the impact of controls implementation is not much effective. The number of recoveries take a bow-down after reaching a peak. However, when immunity loss rate is less, i.e., $r = 0.0002$, the number of recoveries is highest and attains a saturation level, indicating the limitations of the healthcare system.

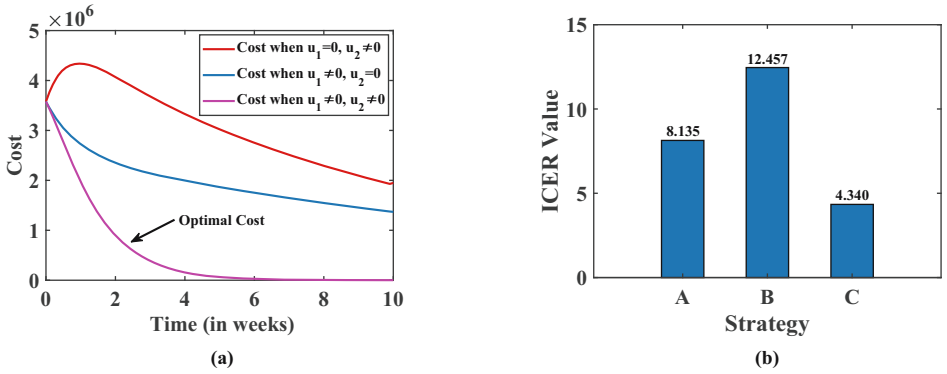

Figure 17: (a) The cost profiles and (b) ICER values, for different strategies.

4.5 Cost-efficacy analysis

The main objective of CEA is to determine the intervention or strategy that yields the maximum health benefit at the lowest cost. CEA is commonly utilized to guide decision-making in allocating resources for public health programs and policies. There are three main techniques for this analysis [1,37]: averted infections ratio, average cost-effectiveness ratio, and incremental cost-effectiveness ratio (ICER). For our purpose, we will employ the ICER method.

The ICER is a metric that measures the cost required to produce an additional unit of health outcome, and it allows for a comparison of the efficiency of different strategies in incremental terms. This metric is used to compare an intervention with the next less efficient alternative, and so on, until the most cost-efficient intervention is determined. By using ICER, it becomes possible to assess and compare different strategies, usually two or more, and make informed decisions about trade-offs between costs and health outcomes. The ICER formula [1] can be written as follows:

$$\text{ICER} = \frac{\text{Cost}_j - \text{Cost}_k}{\text{Effectiveness}_j - \text{Effectiveness}_k},$$

where Cost_j and Cost_k represent the costs of two different intervention strategies, and Effectiveness_j and Effectiveness_k represent their corresponding health outcomes or effectiveness. The ICER calculates the ratio of the difference in costs to the difference in effectiveness between the two strategies, allowing for a comparison of their relative cost-effectiveness. The policy with the lowest ICER value is considered to be the most cost-effective in terms of both disease prevalence and the cost associated with implementing control measures. The cost profiles of various strategies, as compared to the scenario where no control is implemented, are depicted in Figure 17(a). It is evident that the cost (which encompasses both disease burden and economic losses) is significantly higher when no control strategy is employed, as compared to the cases where controls are used. Furthermore, it can be observed that the optimal cost is attained when Strategy C is implemented. The ICER values are obtained for all the strategies and plotted as a bar plot, and the lowest ICER value is attained by the Strategy C. This represents that it is the most cost-effective strategy among all others.

5 Conclusion

To summarize, this article presents an optimal control analysis of COVID-19 interventions in the context of India, incorporating community awareness and immunity loss. We considered a deterministic compartmental S2EI2RS model for COVID-19 transmission with application of controls. We formulated an OCP with two time-dependent controls, namely, home quarantine for exposed and un-notified infectives, and additional treatment effort for notified infectives. In addition, we conducted a basic qualitative analysis of the model, which

included exploring the effects of the controls and community awareness on the reproductive threshold, and determined using the next-generation matrix method. We visualized the results by plotting a surface of R_0 against the controls u_1 and u_2 in the range $[0, 1] \times [0, 1]$. Our findings indicate that the full efforts of applying both controls ($u_1 = 1 = u_2$) simultaneously achieve the lowest value of R_0 (0.0918) compared to other scenarios, suggesting that this approach is most effective in achieving a disease-free environment. We investigated the impact of community awareness on reproduction number in absence of any control, and the results suggest that R_0 is highest when there is less awareness in the community. However, a certain rate of community awareness is required to keep the reproduction number below its threshold, i.e., $R_0 < 1$. The impact of waning immunity on the recoveries is also studied in absence of any control, the results indicate that lowering the rate if immunity loss can be very much helpful in increasing number of recovered individuals.

The necessary and sufficient conditions for the existence and characterization of the optimality system were proven, and we solved the OCP using PMP and the FBSM. We conducted numerical simulations using MATLAB and analyzed the application of controls by considering their individual and combined implementation. It is noted that implementation of only u_1 (home quarantine) is helpful in reducing the number of infective counts, which eventually reduces the load on the treatment, while the use of only u_2 (additional treatment effort) impacts better than only u_1 for notified infectives. But the simultaneous application of both control strategies is the most optimal and sustainable way to reduce the disease burden in a short period of time. The ICERs also suggest the same. In addition, when examining the numerical simulation of the removed population, it is observed that utilizing both control measures simultaneously results in a saturation point after around 35 days, suggesting a scarcity of healthcare and economic resources. This finding may inspire researchers to investigate the impact of limited medical facilities, particularly in developing countries, on this saturation phenomenon. In addition, we have examined the influence of immunity loss on the number of individuals who recover when both controls ($u_1 \neq 0 \neq u_2$) are implemented simultaneously. The results demonstrate that when the rate of immunity loss is high, the effectiveness of control measures is relatively limited. The number of recoveries initially increases but eventually declines after reaching a peak. However, when the rate of immunity loss is lower, specifically at $r = 0.0002$, the number of recoveries reaches its highest level and stabilizes, highlighting once again the constraints of the healthcare system.

This research contributes to the existing literature in several significant ways. Firstly, we have considered a S2EI2RS type deterministic compartmental model of COVID-19, which incorporates awareness at susceptibility level unlike most of the other existing models. This enables a more comprehensive and meaningful understanding of disease dynamics and control strategies. Secondly, we have highlighted the effect of controls on reproduction number, which shows impact of using a particular intervention on disease prevalence. Thirdly, our study conducts a cost-effective optimal control analysis of the OCP formulated by considering home quarantine as an intervention for exposed and un-notified infective individuals and additional treatment efforts for notified individuals, providing valuable insights for policymakers and public health experts in designing targeted and efficient interventions for COVID-19 and future epidemics. We believe that the combination of these novel elements makes our research unique and impactful in addressing the challenges posed by infectious diseases.

Our study provides important insights on optimal control strategies that account for community awareness and immunity loss into the model for controlling the spread of COVID-19. These findings can be instrumental in guiding policymakers and public health experts towards implementing more targeted and effective control measures for not only COVID-19 but also future epidemics in the post-COVID era. By doing so, we can prevent the spread of infectious diseases, save lives, and create a more resilient public health system.

Acknowledgements: SL would like to extend heartfelt thanks to the Ministry of Education, Government of India, for generous support through the Prime Minister's Research Fellows (PMRF) scheme [PMRF ID: 2701459]. The authors are thankful the anonymous referees for their constructive suggestions which has significantly improved the manuscript.

Funding information: This research received no specific grant from any funding agency, commercial or nonprofit sectors.

Author contributions: Sonu Lamba conceived the idea, performed analysis and computation, wrote, and reviewed the draft. Prashant K. Srivastava discussed the idea and supervised, wrote, and reviewed the draft.

Conflict of interest: The authors state that they have no competing interests to declare and have not engaged in any other activities that may pose a perceived conflict of interest.

Ethical approval: This research did not required ethical approval.

References

[1] Agusto, F. B., & ELmojtaba, I. M. (2017). Optimal control and cost-effective analysis of malaria/visceral leishmaniasis co-infection. *PLoS One*, *12*(2), e0171102.

[2] Arbane, M., Benlamri, R., Brik, Y., & Alahmar, A. D. (2023). Social media-based covid-19 sentiment classification model using bi-lstm. *Expert Systems with Applications*, *212*, 118710.

[3] Asamoah, J. K. K, Owusu, M. A., Jin, Z., Oduro, F. T., Abidemi, A., & Gyasi, E. O. (2020). Global stability and cost-effectiveness analysis of covid-19 considering the impact of the environment: using data from ghana. *Chaos, Solitons & Fractals*, *140*, 110103.

[4] Batistela, C. M., Correa, D. P. F., Bueno, A. M., & Piqueira, J. R. C. (2021). Sirsi compartmental model for covid-19 pandemic with immunity loss. *Chaos, Solitons & Fractals*, *142*, 110388.

[5] Chang, X., Liu, M., Jin, Z., & Wang, J. (2020). Studying on the impact of media coverage on the spread of covid-19 in Hubei province, China. *Mathematical Biosciences and Engineering*, *17*(4), 3147–3159.

[6] Coddington, E. A., Levinson, N., & Teichmann, T. (1956). Theory of ordinary differential ėquations. *Physics Today*, *9*(2), 18.

[7] Ferry, A. V., Keanie, C., Denvir, M. A., Mills, N. L., & Strachan F. E.. (2021). Chest pain presentations to hospital during the covid-19 lockdown: Lessons for public health media campaigns. *PLoS One*, *16*(4), e0249389.

[8] Fleming, W. H., & Rishel, R. W. (2012). *Deterministic and stochastic optimal control*, (Vol. 1). New York: Springer Verlag.

[9] Ghosh, I., & Martcheva, M. (2021). Modeling the effects of prosocial awareness on covid-19 dynamics: Case studies on Colombia and India. *Nonlinear Dynamics*, *104*(4), 1–20.

[10] Ghosh, S. K., & Ghosh, S. (2023). A mathematical model for covid-19 considering waning immunity, vaccination and control measures. *Scientific Reports*, *13*(1), 3610.

[11] James, L. P., Salomon, J. A., Buckee, C. O., & Menzies, N. A. (2021). The use and misuse of mathematical modeling for infectious disease policymaking: lessons for the covid-19 pandemic. *Medical Decision Making*, *41*(4), 379–385.

[12] Juneau, C.-E., Briand, A.-S., Collazzo, P., Siebert, U., & Pueyo, T. (2023). Effective contact tracing for covid-19: A systematic review. *Global Epidemiology*, *5*, 100103.

[13] Khan, M. A., & Atangana, A. (2022). Mathematical modeling and analysis of covid-19: A study of new variant omicron. *Physica A: Statistical Mechanics and its Applications*, *599*, 127452.

[14] Kifle, Z. S., & Obsu, L. L. (2022). Mathematical modeling for covid-19 transmission dynamics: A case study in ethiopia. *Results in Physics*, *34*, 105191.

[15] Kobe, F. T., & Koya, P. R. (2020). Modeling and analysis of effect of awareness programs by media on the spread of covid-19 pandemic disease. *American Journal of Applied Mathematics*, *8*(4), 223–229.

[16] Kucharski, A. J., Russell, T. W., Diamond, C., Liu, Y., Edmunds, J., Funk, S., ..., Davies, N. (2020). Early dynamics of transmission and control of covid-19: a mathematical modelling study. *The Lancet Infectious Diseases*, *20*(5), 553–558.

[17] Kumar, A., & Srivastava, P. K. (2017). Vaccination and treatment as control interventions in an infectious disease model with their cost optimization. *Communications in Nonlinear Science and Numerical Simulation*, *44*, 334–343.

[18] Lakshmikantham, V., Leela, S., & Martynyuk, A. A. (1989). *Stability Analysis of Nonlinear Systems*. Switzerland: Springer International Publishing.

[19] Lenhart, S., & Workman, J. T. (2007). *Optimal control applied to biological models*. New York: CRC.

[20] Li, M. L., Bouardi, H. T., Lami, O. S., Trikalinos, T. A., Trichakis, N., Bertsimas, D. (2023). Forecasting covid-19 and analyzing the effect of government interventions. *Operations Research*, *71*(1), 184–201.

[21] Linton, N. M., Kobayashi, T., Yang, Y., Hayashi, K., Akhmetzhanov, A. R., Jung, S., ..., Nishiura, H. (2020). Incubation period and other epidemiological characteristics of 2019 novel coronavirus infections with right truncation: a statistical analysis of publicly available case data. *Journal of Clinical Medicine*, *9*(2), 538.

[22] López, L., & Rodó, X. (2020). The end of social confinement and covid-19 re-emergence risk. *Nature Human Behaviour*, *4*(7), 746–755.

[23] Mandal, S., Bhatnagar, T., Arinaminpathy, N., Agarwal, A., Chowdhury, A., Murhekar, M., ..., Sarkar, S. (2020). Prudent public health intervention strategies to control the coronavirus disease 2019 transmission in india: A mathematical model-based approach. *The Indian Journal of Medical Research*, *151*(2–3), 190.

[24] McAsey, M., Mou, L., & Han, W. (2012). Convergence of the forward-backward sweep method in optimal control. *Computational Optimization and Applications*, *53*(1), 207–226.
[25] Mohsen, A. A., Al-Husseiny, H. F., Zhou, X., & Hattaf, K. (2020). Global stability of covid-19 model involving the quarantine strategy and media coverage effects. *AIMS Public Health*, *7*(3), 587.
[26] Musa, S. S., Qureshi, S., Zhao, S., Yusuf, A., Mustapha, T. U., & He, D. (2021). Mathematical modeling of covid-19 epidemic with effect of awareness programs. *Infectious Disease Modelling*, *6*, 448–460.
[27] Pan, A., Liu, L., Wang, C., Guo, H., Hao, X., Wang, Q., ..., Wei, S. (2020). Association of public health interventions with the epidemiology of the covid-19 outbreak in Wuhan, *China. Jama*, *323*(19), 1915–1923.
[28] Prem, K., Liu, Y., Russell, T. W., Kucharski, A. J., Eggo, R. M., Davies, N., ..., Abbott, S. (2020). The effect of control strategies to reduce social mixing on outcomes of the covid-19 epidemic in Wuhan, China: a modelling study. *The Lancet Public Health*, *5*(5), e261–e270.
[29] Saha, S., Samanta, G. P., & Nieto, J. J. (2020). Epidemic model of covid-19 outbreak by inducing behavioural response in population. *Nonlinear Dynamics*, *102*, 455–487.
[30] Samanta, S., Rana, S., Sharma, A., Misra, A. K., & Chattopadhyay, J. (2013). Effect of awareness programs by media on the epidemic outbreaks: A mathematical model. *Applied Mathematics and Computation*, *219*(12), 6965–6977.
[31] Sardar, T., Nadim, S. S., Rana, S, & Chattopadhyay, J. (2020). Assessment of lockdown effect in some states and overall india: A predictive mathematical study on covid-19 outbreak. *Chaos, Solitons & Fractals*, *139*, 110078.
[32] Srivastava, A., Sonu, & Srivastava, P. K. (2022). Nonlinear dynamics of a siri model incorporating the impact of information and saturated treatment with optimal control. *The European Physical Journal Plus*, *137*(9), 1–25.
[33] Srivastav, A. K., Tiwari, P. K., Srivastava, P. K., Ghosh, M., & Kang, Y. (2021). A mathematical model for the impacts of face mask, hospitalization and quarantine on the dynamics of covid-19 in india: deterministic vs. stochastic, *Mathematical Biosciences and Engineering*, *18*(1), 182–213.
[34] Tindale, L. C., Coombe, M., Stockdale, J. E., Garlock, E. S., Venus Lau, W. Y., Saraswat, M., ..., Colijn, C. (2020). *Transmission interval estimates suggest pre-symptomatic spread of covid-19*. MedRxiv, 2020–03.
[35] Tiwari, P. K., Rai, R. K., Khajanchi, S., Gupta, R. K., & Misra, A. K. (2021). Dynamics of coronavirus pandemic: effects of community awareness and global information campaigns. *The European Physical Journal Plus*, *136*(10), 994.
[36] Van den Driessche, P., & Watmough, J. (2002). Reproduction numbers and sub-threshold endemic equilibria for compartmental models of disease transmission. *Mathematical Biosciences*, *180*(1–2), 29–48.
[37] Weinstein, M. C., Russell, L. B., Gold, M. R., Siegel, J. E. (1996). *Cost-effectiveness in health and medicine*. New York: Oxford University Press.
[38] Wu, Z., & McGoogan, J. M. (2020). Characteristics of and important lessons from the coronavirus disease 2019 (covid-19) outbreak in china: summary of a report of 72 314 cases from the chinese center for disease control and prevention. *Jama*, *323*(13), 1239–1242.
[39] Zhou, W., Wang, A., Xia, F., Xiao, Y., & Tang, S. (2020). Effects of media reporting on mitigating spread of covid-19 in the early phase of the outbreak. *Mathematical Biosciences and Engineering*, *17*(3), 2693–2707.